Journal of Inorganic and Organometallic Polymers and Materials
https://doi.org/10.1007/s10904-025-04066-y

RESEARCH

Neutral Manganese(II) Chloride Scintillators with Phosphine Oxide Ligands Featuring Large Steric Hindrance for X-Ray Imaging

Xiaokang Zheng[1,2,3] · Zikang Li[2] · Peng Tao[2,3] · Hua Wang[1,4] · Lijie Zhang[5] · Wai-Yeung Wong[2,3]

Received: 6 September 2025 / Accepted: 23 September 2025

Abstract

Although organic-inorganic manganese(II) halides have achieved significant advancements, research on the relationship among their structure, photophysical properties, and scintillation performance remains understudied, especially in neutral manganese(II) chlorides. In this work, we design and synthesize three neutral manganese(II) chlorides ((1-*t*Bu)$_2$MnCl$_2$, (2-*t*Bu)$_2$MnCl$_2$, and (3-*t*Bu)$_2$MnCl$_2$) by incorporating phosphine oxide ligands with tunable steric hindrance. Interestingly, the photoluminescence quantum yields (PLQYs) of these green emissive complexes are highly dependent on the combinations of the benzene ring and *tert*-butyl (*t*Bu) group, resulting in the PLQYs in the range of 1.7% to 55.6%. The PLQY of (2-*t*Bu)$_2$MnCl$_2$ represents the highest value up to 55.6% among neutral monodentate manganese(II) chlorides. The rigidity of the benzene ring and steric hindrance of the *t*Bu groups effectively suppress the non-radiative transition processes under UV excitation. Notably, as the X-ray scintillator, (1-*t*Bu)$_2$MnCl$_2$ and (2-*t*Bu)$_2$MnCl$_2$ exhibit high light yields of 13021.7 photons/MeV and 14562.3 photons/MeV, respectively, with a spatial resolution exceeding 10 lp/mm for X-ray imaging. This work demonstrates the rational design of the of *t*Bu-modified manganese(II) chlorides as the efficient luminescent materials for scintillators, thereby paving the way for the development of high-performance neutral monodentate manganese(II) complexes.

Graphical Abstract

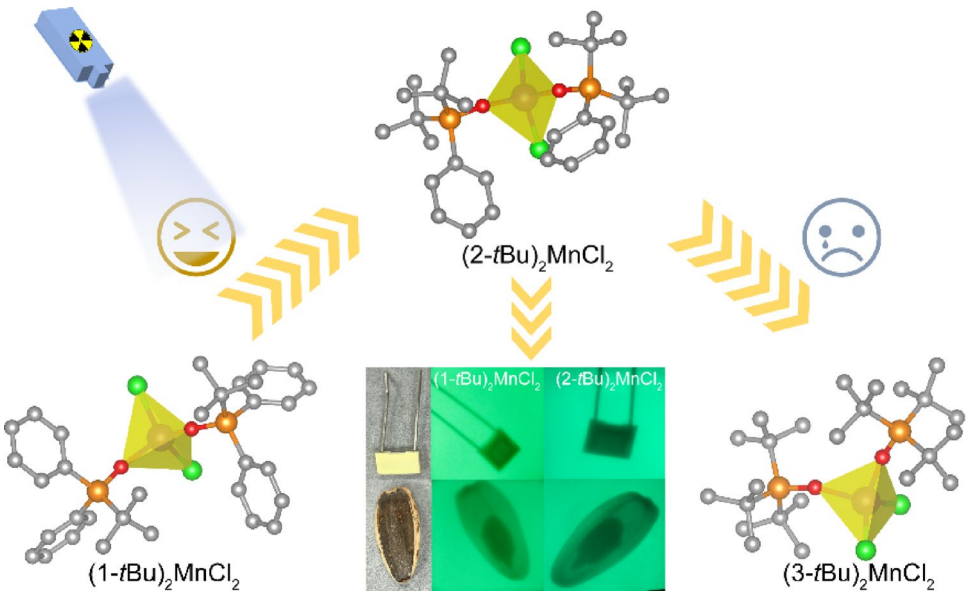

Keywords Organic-inorganic hybrid halide · Manganese(II) chloride · Scintillator · Steric hindrance · X-ray imaging

Extended author information available on the last page of the article

Published online: 19 October 2025

1 Introduction

X-ray imaging is essential to disease diagnosis and therapeutic monitoring, enabling real-time assessment of treatment efficacy and disease progression [1–3]. As the promising low-temperature processable scintillator materials, organic-inorganic manganese(II) halides have garnered extensive attention owing to their excellent performance in X-ray imaging, particularly for high-resolution medical diagnostics and industrial inspection [4–10]. Especially for manganese(II) bromides, they often show higher light yields (LYs) and spatial resolution than some of the traditional inorganic scintillators (e.g. BGO, BaF_2, and LuAG:Ce) that suffer from high metal toxicity, high cost, and stringent preparation conditions [11–14]. For instance, (4-DEATBP)$MnBr_4$ (4-DEATBP = 4-(diethylamino)butyl) triphenylphosphonium), $(C_{20}H_{20}P)_2MnBr_4$ ($C_{20}H_{20}P$ = ethyltriphenylphosphonium) and $(BTPP)_2MnBr_4$ (BTPP = benzyltriphenylphosphonium) in different film states such as flexible film, glass or innogel have been studied with high photoluminescence quantum yields (PLQYs) ranging from 47% to 100% and spatial resolution ranging from 14.1 lp/mm to 25 lp/mm, meeting the requirements of medical imaging detectors [15–17].

However, manganese(II) halides are currently dominated by bromine-containing complexes, as previous studies have emphasized the importance of heavy halogen atoms in enhancing the PLQYs and the X-ray imaging performance of scintillators [18–22]. In contrast, the development of chlorine-based manganese(II) scintillators, particularly neutral monodentate manganese(II) chloride scintillators remains limited. In general, neutral manganese(II) chlorides exhibit lower PLQYs (< 30%), LYs (< 10000 photons/MeV) and spatial resolution (< 10 lp/mm) compared to their ionic counterparts. This is attributed to the weaker spin-orbit coupling and higher ligand field strength associated with chlorine [23–26]. Given the limited research on neutral chloride-based manganese(II) complexes, there is no sufficient evidence to establish the correlation among PLQY, LY, and spatial resolution. Enhancing the PLQYs of X-ray scintillators has been demonstrated as a crucial strategy for increasing their LYs [27–31]. Therefore, regulating the PLQYs of neutral monodentate manganese(II) chlorides through rational molecular design is essential for achieving high-performance X-ray imaging.

Herein, we explored the structure-property relationships of neutral manganese(II) chlorides ($(1\text{-}t\text{Bu})_2MnCl_2$, $(2\text{-}t\text{Bu})_2MnCl_2$, and $(3\text{-}t\text{Bu})_2MnCl_2$) by incorporating phosphine oxide ligands with varying degrees of steric hindrance. These complexes exhibited green emission with tunable PLQYs of 36.1%, 55.6%, and 1.7%, respectively. The steric hindrance of *tert*-butyl (*t*Bu) groups can modulate the lattice distortion and electronic band structures of these complexes by varying the number of *t*Bu groups, thereby influencing the ligand field strengths. The design strategy of balancing rigidity with flexibility by regulating the number of *t*Bu groups and benzene rings also aims at the suppression of non-radiative transitions to enhance PLQY. Compared with $(1\text{-}t\text{Bu})_2MnCl_2$, $(2\text{-}t\text{Bu})_2MnCl_2$ not only showed a higher PLQY but also exhibited thermally activated luminescence from 100 K to 220 K. Owing to the high PLQYs of $(1\text{-}t\text{Bu})_2MnCl_2$ and $(2\text{-}t\text{Bu})_2MnCl_2$, their LYs were determined to be up to 13021.7 photons/MeV and 14562.3 photons/MeV. Furthermore, $(1\text{-}t\text{Bu})_2MnCl_2$ and $(2\text{-}t\text{Bu})_2MnCl_2$ achieved the low detection limits (LODs) of 0.310 μGy/s and 0.153 μGy/s and high spatial resolution of 10.3 lp/mm and 12.4 lp/mm, respectively. These results demonstrated that the *t*Bu group modification-based design strategy for manganese(II) complexes represented an efficient approach for tuning the excited state of neutral monodentate manganese(II) chloride scintillator materials.

2 Experimental Section

Synthesis of $(1\text{-}t\text{Bu})_2MnCl_2$: *tert*-Butyldiphenylphosphine (5 g) was dissolved in 50 mL CH_2Cl_2 at 0 °C, and 20 mL H_2O_2 was added dropwise to the mixture. After stirring for 12 h, the mixture was extracted three times with CH_2Cl_2. After that, the ligand was obtained from the organic phase as a white powder via rotary evaporation without any additional purification. Ligand (1.5 g, 6 mmol) was dissolved in CH_2Cl_2 and $MnBr_2{\cdot}4H_2O$ (0.86 g, 3 mmol) was dissolved in ethanol (EtOH). The EtOH solution was added to the CH_2Cl_2 solution of ligand, and the mixture was stirred at room temperature for 12 h. After that, the precipitated compound was filtered, washed with ethyl acetate (EA), and dissolved in CH_2Cl_2. Finally, green crystals of $(1\text{-}t\text{Bu})_2MnCl_2$ were obtained by slow evaporation of CH_2Cl_2 and EA mixed solution at room temperature in air (Yield: 81%).

Synthesis of $(2\text{-}t\text{Bu})_2MnCl_2$: $(2\text{-}t\text{Bu})_2MnCl_2$ was synthesized by the same procedure as $(1\text{-}t\text{Bu})_2MnCl_2$. Green crystals of $(2\text{-}t\text{Bu})_2MnCl_2$ were obtained by slow evaporation of CH_2Cl_2 and EA mixed solution at room temperature in air (Yield: 93%).

Synthesis of $(3\text{-}t\text{Bu})_2MnCl_2$: *Tris*(1,1-dimethylethyl) phosphine oxide (1.5 g, 7 mmol) was dissolved in CH_2Cl_2 and $MnBr_2{\cdot}4H_2O$ (0.99 g, 3.5 mmol) was dissolved in EtOH. The EtOH solution was added to the CH_2Cl_2 solution of *tris*(1,1-dimethylethyl)phosphine oxide, and the mixture was stirred at room temperature for 12 h. After that, the precipitated compound was dissolved in CH_2Cl_2. Finally, green crystals of $(3\text{-}t\text{Bu})_2MnCl_2$ were obtained by evaporation of

CH_2Cl_2 and EA mixed solution at room temperature in air (Yield: 30%).

3 Results and Discussion

Single crystals of (1-*t*Bu)$_2$MnCl$_2$, (2-*t*Bu)$_2$MnCl$_2$, and (3-*t*Bu)$_2$MnCl$_2$ were obtained *via* the solvent evaporation method using a mixed solvent of CH_2Cl_2 and EtOH. The single crystals of these complexes appear as green, transparent crystals under room light and exhibit green luminescence under UV light. As shown in Fig. 1a, their crystal structures were confirmed by single-crystal X-ray diffraction. The detailed crystallographic data were summarized in Tables S1 and S2. Crystal structure analysis suggested that (1-*t*Bu)$_2$MnCl$_2$ crystallized in orthorhombic *Pbca*, while (2-*t*Bu)$_2$MnCl$_2$ and (3-*t*Bu)$_2$MnCl$_2$ crystallized in monoclinic *C*2/*c* and *P*2$_1$/*n*, respectively. All these complexes were 0D neutral monodentate manganese(II) chlorides consisting of two phosphine oxide ligands and a [$MnCl_2$] moiety. The key difference among these complexes was the number of *t*Bu groups within the ligands. The steric hindrance of *t*Bu groups not only isolates the Mn^{2+} centers but also regulates the packing of Mn(II) tetrahedra in the crystal, thereby finely-tuning the Mn-Mn distances. The Mn(II) tetrahedra adopt different packing modes due to the variation in the number of sterically hindered groups, leading to their shortest Mn-Mn distances of 9.493 Å, 8.167 Å, and 8.637 Å, respectively (Figure S1).

These complexes were further characterized by powder X-ray diffraction (PXRD), Fourier transform infrared (FTIR) spectra, scanning electron microscopy (SEM) and energy dispersive X-ray photoelectron (EDX) spectra. As shown in Fig. 1b, the PXRD patterns showed good agreement between experimental and simulated data, implying high phase purity of these complexes. FTIR spectra of these complexes in Figure S2 exhibited similar absorption peaks. The vibrational peaks at around 3000 cm^{-1} were attributed to C-H bonds, and those at around 1200 cm^{-1} arose from P=O bonds, confirming the presence of phosphine oxide ligands in crystal. The SEM-EXD spectra shown in Fig. 1c also confirmed the presence of P, Mn, and Cl elements. Additionally, thermogravimetric analysis (TGA) was employed to evaluate the thermal stability of these complexes. The onset decomposition temperatures of weight loss at 5% are determined to be 272.2 °C for (1-*t*Bu)$_2$MnCl$_2$, 285.2 °C for (2-*t*Bu)$_2$MnCl$_2$ and 288.8 °C for (3-*t*Bu)$_2$MnCl$_2$, respectively (Figure S3).

To explore the luminescence behavior of these complexes, their photophysical properties were characterized (Fig. 2, Table S3). As shown in Fig. 2a, the as-prepared crystals displayed green emission under 365 nm UV-light. The steady-state excitation (PLE) spectra exhibited three excitation bands (250–300 nm, 320–400 nm, and 400–500 nm), which can be ascribed to $^6A_1 \rightarrow {}^4G$, $^6A_1 \rightarrow {}^4D$, ^4P, and $^6A_1 \rightarrow {}^4F$ transitions of Mn ions (Fig. 2b). The photoluminescence (PL) spectra of these complexes, depicted in Fig. 2c, were centered at 527 nm, 507 nm, and 510 nm, respectively. These results indicated that the Mn^{2+} ions were situated within differing crystal field (CF) strengths, which are influenced by the *t*Bu-modified ligands. This finding further confirmed that *t*Bu-modified ligands can influence the luminescence wavelength of manganese(II) complexes by modulating the $^4T_1$ level of Mn^{2+} [32]. The PLQYs of these complexes were measured as 30.1%, 55.6%, and 1.67%, respectively (Figure S4). In general, the PLQYs of ionic manganese(II) halides typically increase with the shortest Mn-Mn distance [33]. However, our observation ran counter to this principle. The closest Mn-Mn distance (8.167 Å) was observed in (2-*t*Bu)$_2$MnCl$_2$ (Table S4), while the highest PLQY of up to 55.6% was achieved. This result indicated that the PLQYs of the designed complexes were not only related to the Mn-Mn distances but also were influenced by non-radiative transitions regulated by steric hindrance of the ligands.

To further validate this observation, the time-resolved PL decays were characterized, and the results were well-fitted by a single exponential function for these complexes (Fig. 2d). The PL lifetimes of these complexes were calculated to be 1.866 ms, 3.113 ms, and 0.227 ms, respectively. Moreover, the radiative recombination rate constant (k_r) and the non-radiative recombination rate constant (k_{nr}) were calculated and summarized in Table S3. Apparently, (2-*t*Bu)$_2$MnCl$_2$ exhibited an extremely low non-radiative transition rate of only 0.143 ms^{-1}, much lower than that of (3-*t*Bu)$_2$MnCl$_2$. This phenomenon can be attributed to the rapid vibration of C-H bonds of *t*Bu groups under the excitation of UV light, leading to non-radiative recombination. Additionally, the 3D excitation-emission mapping of (3-*t*Bu)$_2$MnCl$_2$ revealed that its emission spectrum varied with the excitation wavelength, indicating the presence of defects or traps. Consequently, (3-*t*Bu)$_2$MnCl$_2$ showed an abnormally low PLQY. In contrast, the 3D excitation-emission mappings of both (1-*t*Bu)$_2$MnCl$_2$ and (2-*t*Bu)$_2$MnCl$_2$ demonstrated that their emissions were originated from the same transition process and there were no extra energy levels [34, 35] To better understand the relationship between the PL and the crystal structure, the bond length distortion (Δd) and bond angle variance (σ^2) in these complexes were calculated and summarized in Table S4. Complex (2-*t*Bu)$_2$MnCl$_2$ exhibited the highest σ^2 (44.1) among these complexes. Notably, adequate steric hindrance can effectively increase lattice distortion, potentially enhancing the luminescence of neutral monodentate manganese(II) chlorides by regulating

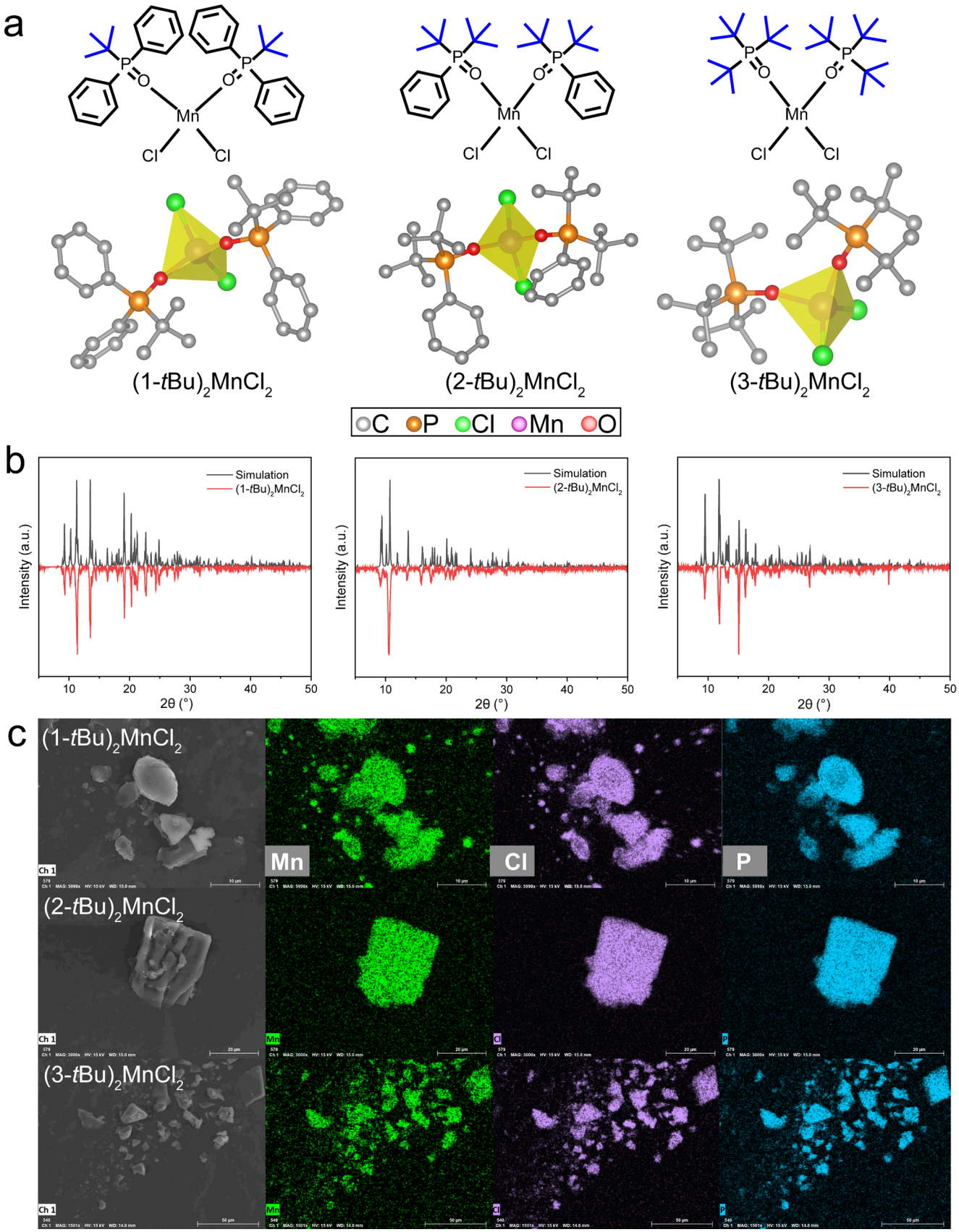

Fig. 1 **a** Chemical drawings and single crystal structures; **b** PXRD patterns; **c** SEM-EDX mappings of $(1\text{-}t\text{Bu})_2MnCl_2$, $(2\text{-}t\text{Bu})_2MnCl_2$, and $(3\text{-}t\text{Bu})_2MnCl_2$

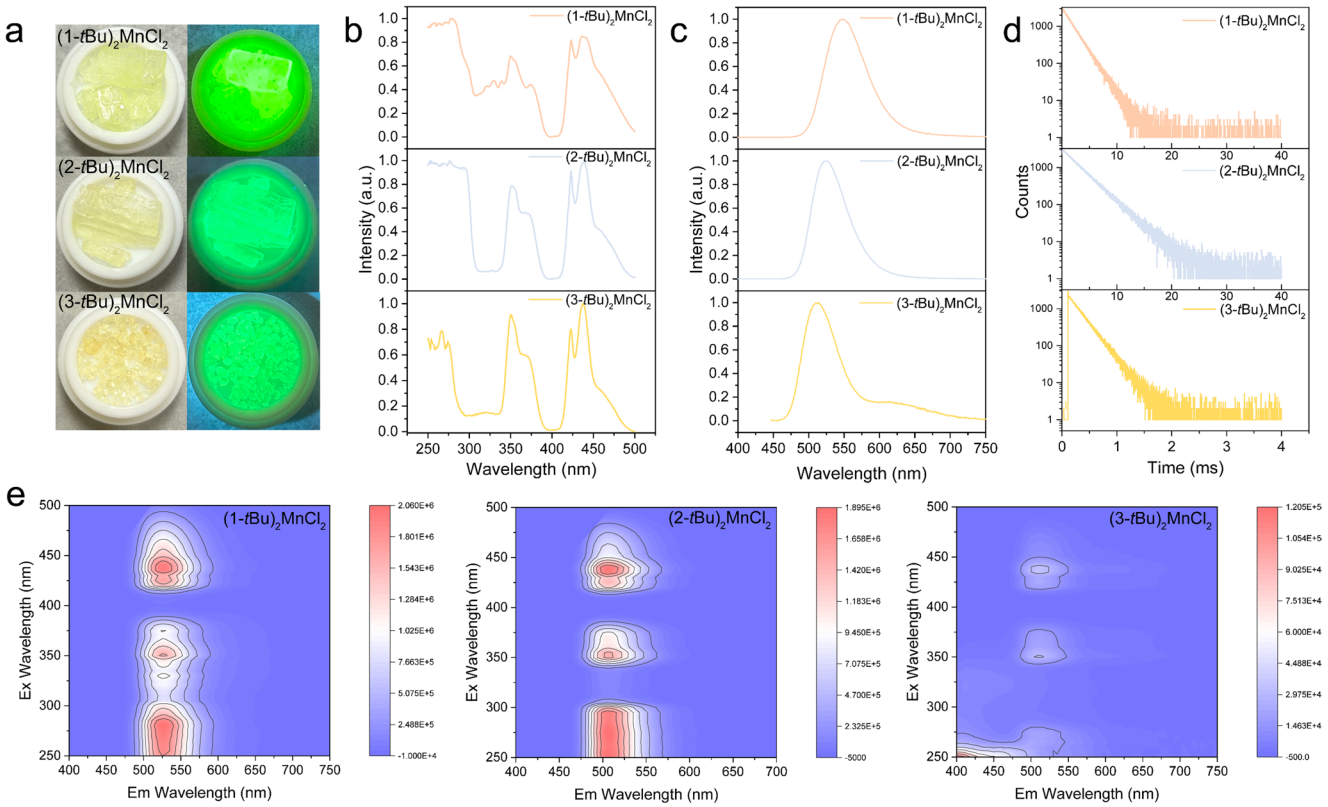

Fig. 2 **a** Photographs under room light and UV light; **b** PLE spectra; **c** PL spectra; **d** PL decay curves; **e** 3D excitation-emission mappings of (1-*t*Bu)$_2$MnCl$_2$, (2-*t*Bu)$_2$MnCl$_2$, and (3-*t*Bu)$_2$MnCl$_2$ crystals

electron-phonon coupling and suppressing non-radiative transitions.

Considering the extremely low PLQY of (3-*t*Bu)$_2$MnCl$_2$, temperature-dependent PL (TDPL) measurements were performed for (1-*t*Bu)$_2$MnCl$_2$ and (2-*t*Bu)$_2$MnCl$_2$ to gain deeper insights into the luminescence mechanism of neutral monodentate manganese(II) chlorides (Figs. 3, and S5). As shown in Fig. 3a and d, the PL intensity of (1-*t*Bu)$_2$MnCl$_2$ and (2-*t*Bu)$_2$MnCl$_2$ decreased as the temperature increased from 100 K to 300 K as well as the FWHMs gradually increased. The increase in FWHM with increasing temperature was attributed to the electron-phonon coupling effects that deactivated the excitation [36]. Both complexes exhibited a slight red-shift as the temperature decreased, which could be attributed to the thermal-induced lattice expansion of soft lattice of manganese(II) tetrahedra [37–39]. The optical phonon scattering of electrons caused by Fröhlich interaction is also the main reason for the broadening of the FWHM [37]. This may simultaneously facilitate the formation of self-trapped excitons (STEs). Owing to the quantum confinement effect, 0D metal halides easily form self-trapped excitons [40]. To understand the potential STE emission of (1-*t*Bu)$_2$MnCl$_2$ and (2-*t*Bu)$_2$MnCl$_2$, the FWHMs at different temperatures can be fitted using the following equation:

$$\mathrm{FWHM} = 2.36\sqrt{\mathrm{s}}\hbar\omega_{\mathrm{phonon}}\sqrt{\coth\frac{\hbar\omega_{\mathrm{phonon}}}{2k_B\mathrm{T}}}$$

where S is the Huang–Rhys factor, k_B is the Boltzmann constant, and $\hbar\omega_{\mathrm{phonon}}$ is the phonon frequency. The S values of (1-*t*Bu)$_2$MnCl$_2$ and (2-*t*Bu)$_2$MnCl$_2$ were fitted to be 7.74 and 4.36, respectively. The $\hbar\omega_{\mathrm{phonon}}$ values of (1-*t*Bu)$_2$MnCl$_2$ and (2-*t*Bu)$_2$MnCl$_2$ were calculated to be 24.86 meV and 35.3 meV, respectively. Besides, the large σ^2 and long PL lifetimes of (1-*t*Bu)$_2$MnCl$_2$ and (2-*t*Bu)$_2$MnCl$_2$ suggested the presence of the STE emission [41–43]. The small S value of (1-*t*Bu)$_2$MnCl$_2$ and (2-*t*Bu)$_2$MnCl$_2$ suggested the week electron-phonon coupling, which mitigated the thermal luminescence quenching of these complexes [44]. For complex (2-*t*Bu)$_2$MnCl$_2$, the thermally activated luminescence was observed from 100 K to 220 K, and the PL intensity decreased from 220 K to 300 K due to the thermal quenching induced by non-radiative deactivation (Figure S6) [45]. Moreover, the PL intensities of (1-*t*Bu)$_2$MnCl$_2$ and (2-*t*Bu)$_2$MnCl$_2$ showed a linear fit with the increasing excitation power (Figure S7), indicating that the permanent defects could be ruled out [46]. More importantly, the phenyl groups on the ligands not only endowed the complexes with the rigidity but also effectively suppressed the non-radiative transitions. Furthermore, the steric hindrance of

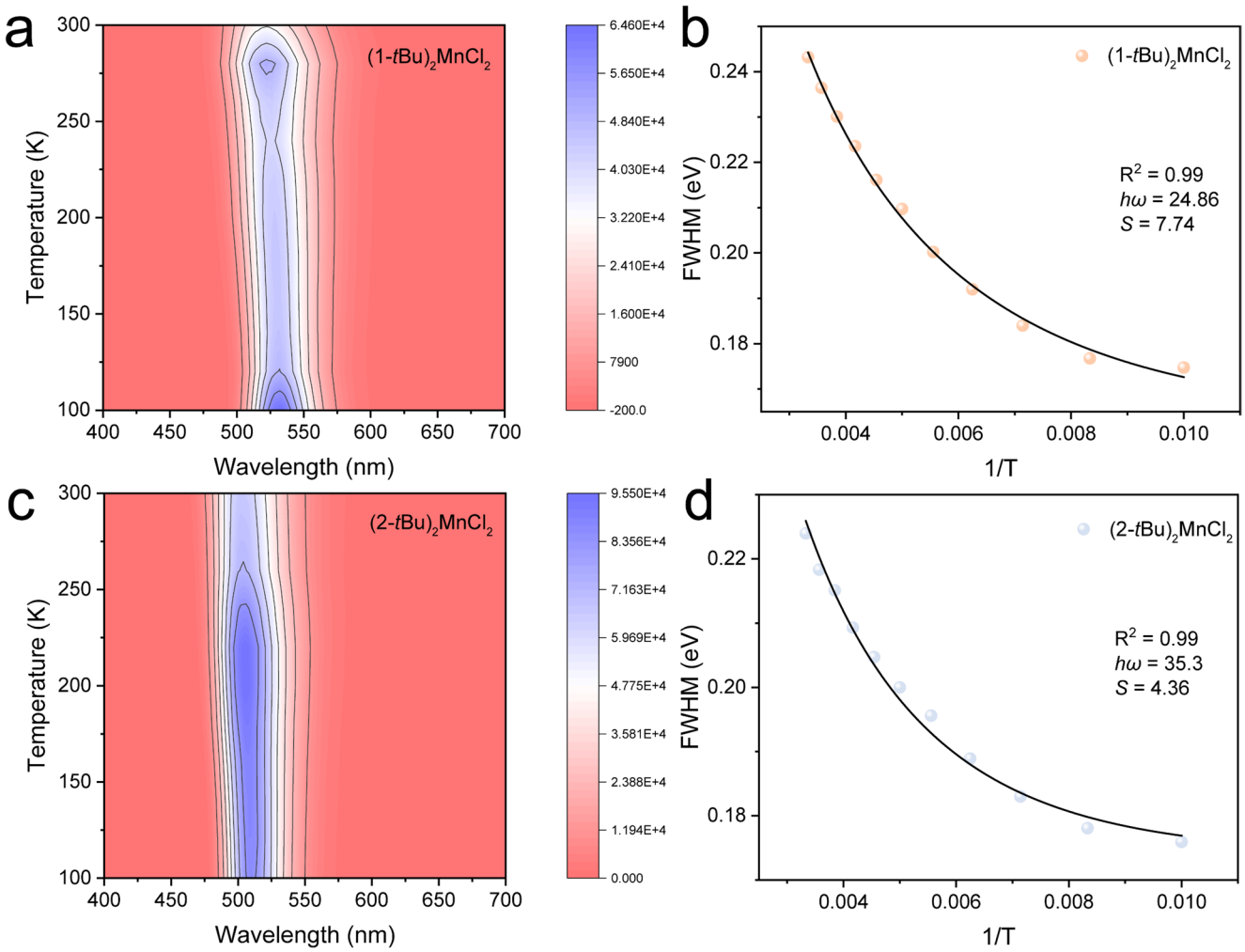

Fig. 3 **a**, **c** The TDPL spectra for (1-*t*Bu)$_2$MnCl$_2$ and (2-*t*Bu)$_2$MnCl$_2$ crystals. **b**, **d** Their FWHM fitting curves as a function of temperature

*t*Bu groups further reduced the concentration quenching in these complexes, resulting in higher PLQY. Compared with the reported complexes (H-Cl and 1-Cl), the *t*Bu-modified neutral monodentate manganese(II) chlorides displayed the superior optical properties (Table S5) [25, 26].

To better understand the electronic structure of these three complexes, density functional theory (DFT) calculations were performed. The density of states (DOS) and band structures were shown in Fig. 4. The band gaps of these complexes were calculated to be 2.406 eV, 2.375 eV, and 3.132 eV, respectively. For complexes (1-*t*Bu)$_2$MnCl$_2$ and (2-*t*Bu)$_2$MnCl$_2$, the valence band maximum (VBM) was composed of Mn d orbitals, Cl p orbitals and ligand p orbitals, while the conduction band minimum (CBM) originated from the ligand p orbitals and Mn d orbitals, suggesting that the charge transfer from ligands to Mn center contributes to the high-efficiency luminescence of (1-*t*Bu)$_2$MnCl$_2$ and (2-*t*Bu)$_2$MnCl$_2$. However, for (3-*t*Bu)$_2$MnCl$_2$, the VBM was composed of Mn d orbitals, while the CBM was originated from the inter-ligand voids in the crystal structure, indicating that the insufficient energy transfer from the ligands to Mn tetrahedra in (3-*t*Bu)$_2$MnCl$_2$ and the severe luminescence quenching induced by the vibration of C-H bonds in *t*Bu groups.

To explore the potential application of (1-*t*Bu)$_2$MnCl$_2$ and (2-*t*Bu)$_2$MnCl$_2$ as scintillator materials, their radioluminescence (RL) properties were further characterized. As shown in Fig. 5a, the absorption coefficients of these complexes were lower than that of commercial scintillators LuAG:Ce due to the lower effective atomic numbers (Z_{eff}). In addition, the X-ray attenuation efficiency plots of (1-*t*Bu)$_2$MnCl$_2$ and (2-*t*Bu)$_2$MnCl$_2$ were calculated to be 28.9% and 29.1% at a thickness of 0.1 mm (Figure S8). The LYs of (1-*t*Bu)$_2$MnCl$_2$ and (2-*t*Bu)$_2$MnCl$_2$ were determined to be 13021.7 photons/MeV and 14562.3 photons/MeV (Fig. 5b), surpassing some manganese(II) chloride scintillators [25, 26, 47] Furthermore, the RL intensities of (1-*t*Bu)$_2$MnCl$_2$ and (2-*t*Bu)$_2$MnCl$_2$ increased with a linear

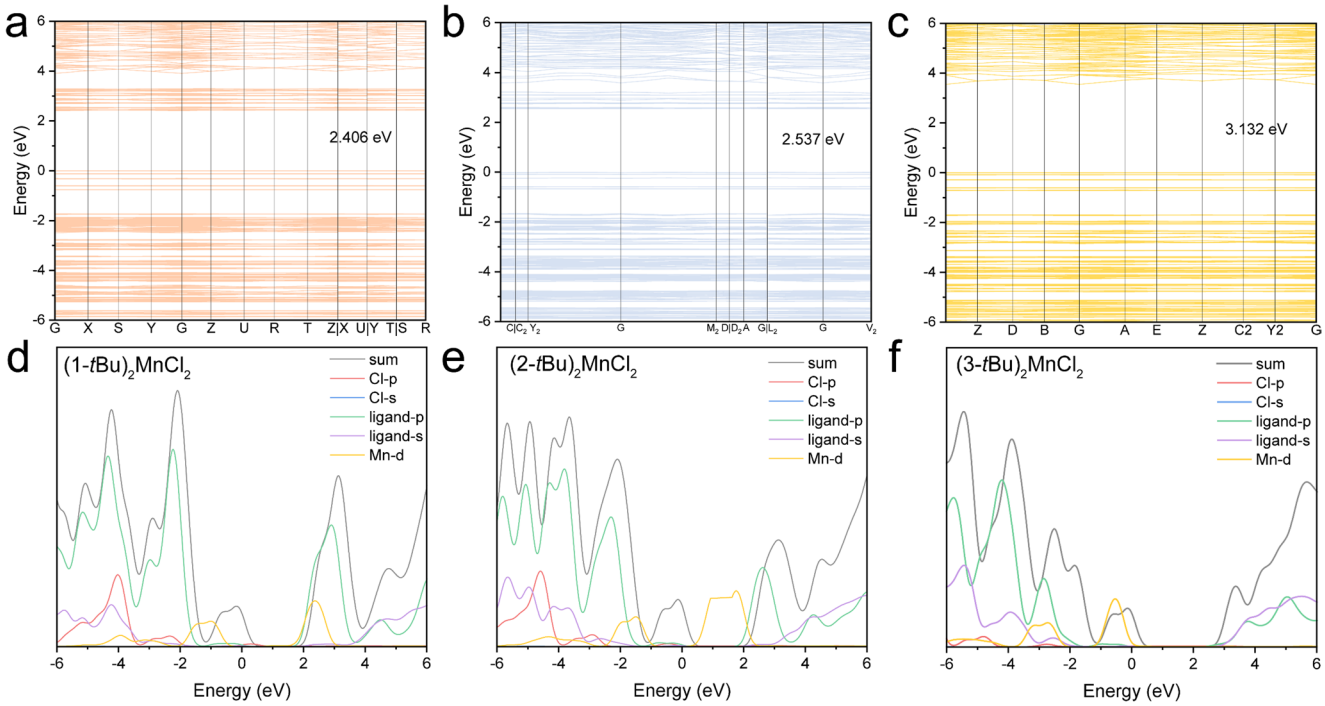

Fig. 4 **a**, **b**, **c** Electronic structure and (**d**, **e**, **f**) DOS analysis for (1-*t*Bu)$_2$MnCl$_2$, (2-*t*Bu)$_2$MnCl$_2$, and (3-*t*Bu)$_2$MnCl$_2$ crystals

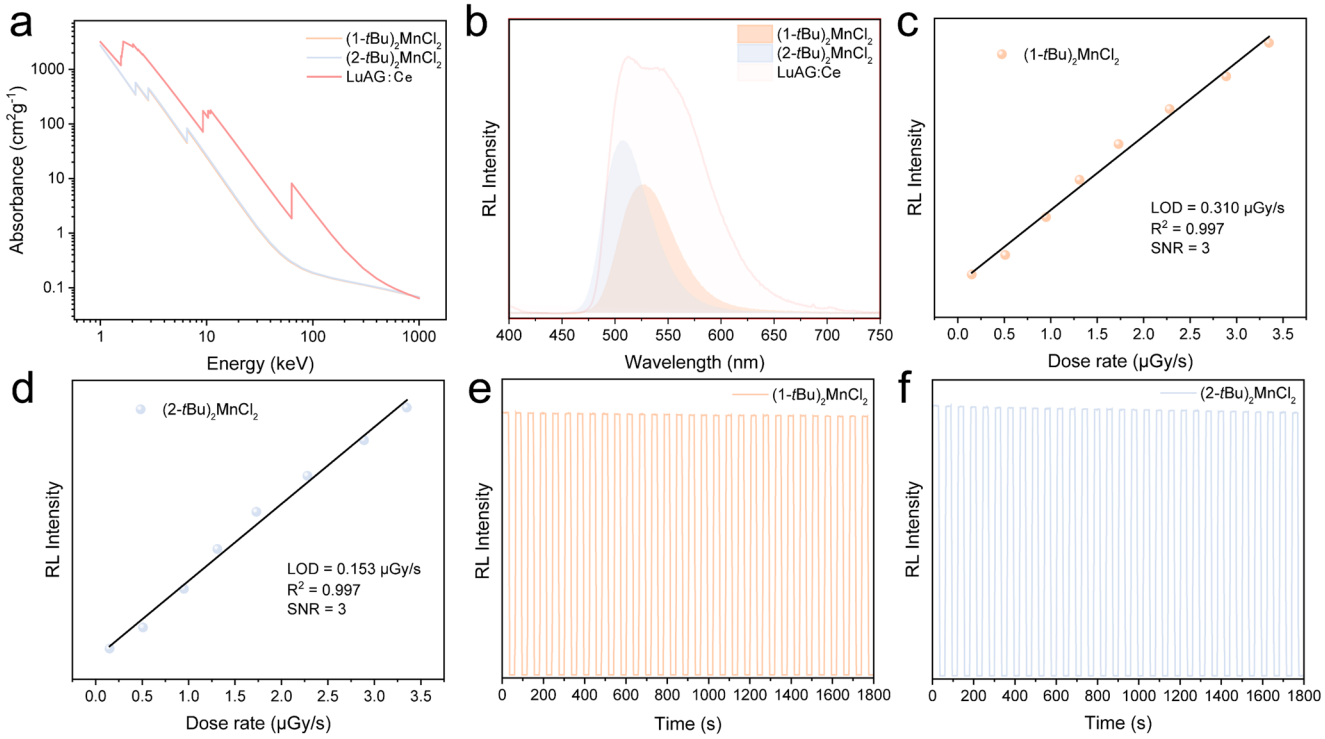

Fig. 5 **a** Absorption coefficients; **b** RL spectra of (1-*t*Bu)$_2$MnCl$_2$ and (2-*t*Bu)$_2$MnCl$_2$. **c**, **d** Linear correlation between RL intensity and X-ray dose rate for (1-*t*Bu)$_2$MnCl$_2$ and (2-*t*Bu)$_2$MnCl$_2$. **e**, **f** The RL stability of (1-*t*Bu)$_2$MnCl$_2$ and (2-*t*Bu)$_2$MnCl$_2$ over 60 continuous on/off cycles at a dose rate of 4.5 mGy/s

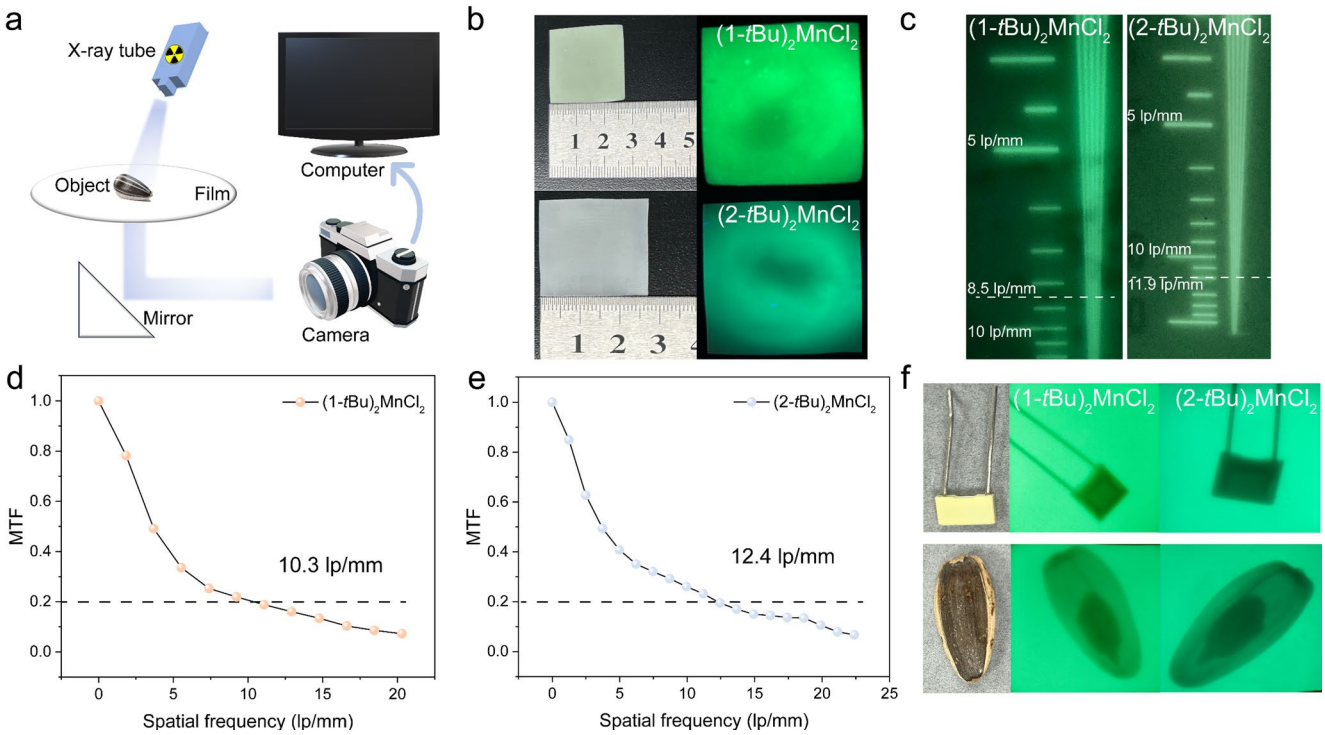

Fig. 6 **a** Schematic of the X-ray imaging system. **b** Photographs of $(1\text{-}t\text{Bu})_2MnCl_2$ and $(2\text{-}t\text{Bu})_2MnCl_2$ film under visible or UV light. **c** X-ray images of the standard line pair card. **d**, **e** MTF curves of $(1\text{-}t\text{Bu})_2MnCl_2$ and $(2\text{-}t\text{Bu})_2MnCl_2$. **f** Bright field images and X-ray images of a sunflower seed and a diode

response to the increasing dose rate from 0.15 μGy/s to 3.35 μGy/s (Fig. 5c and d). After fitting and estimation, the LODs of $(1\text{-}t\text{Bu})_2MnCl_2$ and $(2\text{-}t\text{Bu})_2MnCl_2$ were measured to be 0.310 μGy/s for $(1\text{-}t\text{Bu})_2MnCl_2$ and 0.153 μGy/s for $(2\text{-}t\text{Bu})_2MnCl_2$ at the signal-to-noise ratio (SNR) of 3, which were lower than the diagnostic limit of 5.5 μGy/s [32]. The stability of these complexes under X-ray irradiation at a dose rate of 4.5 mGy/s for 1800 s was also assessed. As shown in Fig. 5e and f, $(1\text{-}t\text{Bu})_2MnCl_2$ and $(2\text{-}t\text{Bu})_2MnCl_2$ exhibited high resistance to X-ray radiation to ensure their applicability in X-ray imaging.

Scintillator films of $(1\text{-}t\text{Bu})_2MnCl_2$ and $(2\text{-}t\text{Bu})_2MnCl_2$ (2.7 cm × 2.7 cm) were further prepared for the X-ray imaging by using a self-built X-ray imaging system as depicted in Fig. 6a. The scintillation films displayed green emission under UV-365 nm light (Fig. 6b). As shown in Fig. 6c, the spatial resolutions for $(1\text{-}t\text{Bu})_2MnCl_2$ and $(2\text{-}t\text{Bu})_2MnCl_2$, with a commercial line pair card used as the object, were approximately 8.5 lp/mm and 11.9 lp/mm, respectively. The modulation transfer functions (MTFs) for $(1\text{-}t\text{Bu})_2MnCl_2$ and $(2\text{-}t\text{Bu})_2MnCl_2$ films, measured *via* the slanted-edge method (Fig. 6d and e), were calculated to be 10.3 lp/mm and 12.4 lp/mm, which is consistent with the results of most manganese(II) chloride scintillators [25, 26, 47–50] To further verify the X-ray imaging performance of these scintillator films, a sunflower seed and a diode were imaged. As depicted in Fig. 6f, both sunflower seed kernel and metal electrodes in diode were clearly visualized at a dose rate of 179 μGy/s. These results clearly demonstrated that the rational design of the *t*Bu-modified manganese(II) chlorides not only can significantly enhance the PLQYs but also improve their RL performance, highlighting their potentials for the flexible X-ray scintillators.

4 Conclusion

In summary, we successfully designed three neutral monodentate manganese(II) chlorides $(1\text{-}t\text{Bu})_2MnCl_2$, $(2\text{-}t\text{Bu})_2MnCl_2$, and $(3\text{-}t\text{Bu})_2MnCl_2$ by incorporating phosphine oxide ligands with tunable steric hindrance. Three complexes exhibited green emission with PLQYs of 30.1% ($(1\text{-}t\text{Bu})_2MnCl_2$), 55.6% ($(2\text{-}t\text{Bu})_2MnCl_2$), and 1.67% ($(3\text{-}t\text{Bu})_2MnCl_2$), respectively. The notable PLQY variations indicated that the design of both rigid structure and sterically hindered ligand is essential for suppressing non-radiative transitions. In addition, the PL of $(1\text{-}t\text{Bu})_2MnCl_2$ and $(2\text{-}t\text{Bu})_2MnCl_2$ was attributed to STE emission, which also explains the anti-thermal quenching of $(2\text{-}t\text{Bu})_2MnCl_2$ within the temperature range from 100 K to 220 K. In terms of RL performance, $(1\text{-}t\text{Bu})_2MnCl_2$ and $(2\text{-}t\text{Bu})_2MnCl_2$ showed high LYs of 13021.7 photons/MeV and 14562.3

photons/MeV, along with LODs of 0.310 μGy/s and 0.153 μGy/s. It is worth noting that the MTF of (1-*t*Bu)$_2$MnCl$_2$ and (2-*t*Bu)$_2$MnCl$_2$ reached 10.3 lp/mmm and 12.4 lp/mm. These values surpassed those of most of the reported manganese(II) chlorides with higher PLQYs. The *t*Bu modification strategy for neutral monodentate manganese(II) chlorides achieves the improvement of PLQYs, LYs, and spatial resolutions for manganese(II) chlorides by regulating the Mn-Mn distance, lattice distortion, and suppressing non-radiative transitions through steric hindrance. This not only facilitates the development of neutral monodentate manganese(II) chloride materials but also provides strong support for the application potential of neutral manganese(II) complexes as high-performance scintillators in orthopedic medical imaging, cultural relics protection, and aerospace fields, thereby further promoting the development of neutral manganese(II) chloride scintillators.

Supplementary Information The online version contains supplementary material available at https://doi.org/10.1007/s10904-025-04066-y.

Acknowledgements We acknowledge the financial support from the National Natural Science Foundation of China (61905120, 52073242, and 62074109), Startup Fund for RAPs under the Strategic Hiring Scheme (P0035922), the Hong Kong Research Grants Council (PolyU 15305320), Research Institute for Smart Energy (CDAQ), Research Centre for Organic Electronics (CE0P), and Miss Clarea Au for the Endowed Professorship in Energy (847S). We also acknowledge Zhejiang International Joint Laboratory of Optical Functional Materials for financial support.

Author Contributions W.-Y. Wong and P. Tao conceived the research and supervised the whole work. X. Zheng conducted the experiments, analyzed the data, and wrote the manuscript with contributions from all authors. Z. Li and L. Zhang carried out the DFT calculations. W.-Y. Wong, P. Tao, and H. Wang revised the manuscript. All authors contributed to the discussion of the results.

Funding Open access funding provided by The Hong Kong Polytechnic University

Data Availability No datasets were generated or analysed during the current study.

Declarations

Conflict of interest These authors declare no conflict of interest.

References

1. W. Shao, X. Wang, Z. Zhang, J. Huang, Z. Han, S. Pi, Q. Xu, X. Zhang, X. Xia, G. Liang, Adv. Opt. Mater. **10**, 2102282 (2022)
2. H. Li, J. Li, S. Shen, S. Chen, H. Wei, B. Xu, Nano. Energy. **119**, 109055 (2024)
3. T. He, W. Shao, J. Yin, H. Wang, Y. Zhou, J.X. Wang, P. Yuan, L.G. Arzaluz, W. Wu, R. Zhou, B. Shao, X. Xia, H. Liang, O.M. Bakr, O.F. Mohammed, Matter 7, 2521–2535 (2024)
4. Q. Meng, L. Zhou, Q. Pang, X. He, T. Wei, J.Z. Zhang, J. Phys. Chem. Lett. **12**, 10204–10211 (2021)
5. J.B. Luo, J.H. Wei, Z.Z. Zhang, Z.L. He, D.B. Kuang, Angew Chem. Int. Ed. **62**, e202216504 (2023)
6. S.B. Xiao, X. Zhang, X. Mao, H.J. Yang, Z.N. Chen, L.J. Xu, Adv. Funct. Mater. **34**, 2404003 (2024)
7. K. Han, K. Sakhatskyi, J. Jin, Q. Zhang, M.V. Kovalenko, Z. Xia, Adv. Mater. **34**, 2110420 (2022)
8. L.J. Xu, X. Lin, Q. He, M. Worku, B. Ma, Nat. Commun. **11**, 4329 (2022)
9. A. Berezin, Mater. Chem. Front. **7**, 2475–2483 (2023)
10. X. Zheng, Z. Zhou, Z. Li, K.Y. Tran, P. She, H. Wang, W.-Y. Wong, Q. Zhao, P. Tao, J. Mater. Chem. C **12**, 8296–8301 (2024)
11. B. Yu, S. Bai, Z. Jia, H. Tang, Y. Liu, H. Liu, Q. Lin, Chem. Mater. **36**, 7921–7928 (2024)
12. W. Shao, G. Zhu, X. Wang, Z. Zhang, H. Lv, W. Deng, X. Zhang, H. Liang, ACS Appl. Mater. Interfaces 2023, 15, 932–941 (2023)
13. Y. Wang, M. Li, Z. Chai, Y. Wang, S. Wang, Angew Chem. Int. Ed. **62**, e202304638 (2023)
14. Z. Feng, H. Cui, Y. Yan, S. Liu, Q. Zhao, Laser Photonics Rev. e00885 (2025)
15. J.H. Chen, J.B. Luo, Q.P. Peng, Z.L. He, J.H. Wei, D.B. Kuang, Angew. Chem. Int. Ed. e202508536 (2025)
16. B. Li, K. Han, Y. Wang, Y. Sun, Z. Xia, Y. Xu, Angew Chem. Int. Ed. **64**, e202502440 (2025)
17. W. Li, Z. Luo, Y. Liu, Y. Wei, X. He, Z. Chen, L. Zhang, Y. Chen, W. Wang, Y. Liu, X. Chang, Z. Quan, Adv. Opt. Mater. **10**, 2102746 (2022)
18. G. Zhou, Z. Liu, J. Huang, M.S. Molokeez, Z. Xiao, C. Ma, Z. Xia, J. Phys. Chem. Lett. **11**, 5956–5962 (2020)
19. P. Tao, S.-J. Liu, W.-Y. Wong, Adv. Opt. Mater. **8**, 2000985 (2020)
20. P. She, Z. Zheng, Y. Qin, F. Li, X. Zheng, D. Zhang, Z. Xie, L. Duan, W.-Y. Wong, Adv. Opt. Mater. **12**, 2302132 (2024)
21. X. Yu, S. Zhong, Z. Guo, J. Guan, H. Tang, X. He, Y. Chen, S. Pan, J. Mater. Chem. C **13**, 2190–2197 (2025)
22. W. Li, Y. Li, Y. Wang, Z. Zhou, C. Wang, Y. Sun, J. Sheng, J. Xiao, Q. Wang, S. Kurosawa, M. Buryi, D. John, K. Paurová, M. Nikl, X. Ouyang, Y. Wu, Laser Photonics Rev. **18**, 2300860 (2024)
23. J. Fan, H. Li, W. Liu, G. Ouyang, Angew Chem. Int. Ed. **64**, e202425661 (2025)
24. Y. Qin, P. She, X. Huang, W. Huang, Q. Zhao, Coord. Chem. Rev. **416**, 213331 (2020)
25. X. Zheng, P. Tao, H. Wang, L. Zhang, W.-Y. Wong, J. Inorg. Organomet. Polym. Mater. (2025). https://doi.org/10.1007/s10904-025-03794-5
26. J. Lu, J. Gao, S. Wang, M.J. Xie, B.Y. Li, W.F. Wang, J.R. Mi, F.K. Zheng, G.C. Guo, Nano. Lett. **23**, 4351–4358 (2023)
27. X. Zheng, P. Tao, H. Wang, W.-Y. Wong, ACS Appl. Opt. Mater. **3**, 942–948 (2025)

28. J. Xu, R. Luo, Z. Luo, J. Xu, Z. Mu, H. Bian, S.Y. Chan, B.Y.H. Tan, D. Chi, Z. An, G. Xing, X. Qin, C. Gong, Y. Wu, X. Liu, Nat. Photonics. **19**, 71–78 (2025)
29. L.Q. Guan, S. Shi, X.W. Niu, S.C. Guo, J. Zhao, T.M. Ji, H. Dong, F.Y. Jia, J.W. Xiao, L.D. Sun, C.H. Yan, Adv. Sci. **9**, 2201354 (2022)
30. Q. Zhou, W. Li, J. Xiao, A. Li, X. Han, Adv. Funct. Mater. **34**, 2402902 (2024)
31. Q. Chen, J. Wu, X. Ou, B. Huang, J. Almutlaq, A.A. Zhumekenov, X. Guan, S. Han, L. Liang, Z. Yi, J. Li, X. Xie, Y. Wang, Y. Li, D. Fan, D.B.L. Teh, A.H. All, O.F. Mohammed, O.M. Bakr, T. Wu, M. Bettinelli, H. Yang, W. Huang, X. Liu, Nature. **561**, 88 (2018)
32. W. Zhang, W. Zheng, L. Li, P. Huang, J. Xu, W. Zhang, Z. Shao, X. Chen, Adv. Mater. **36**, 2408777 (2024)
33. L. Mao, P. Guo, S. Wang, A.K. Cheetham, R. Seshadri, J. Am. Chem. Soc. **142**, 13582–13589 (2020)
34. Y. Cai, S. Yan, X. Du, T. Lin, Y. Lin, L. Qiu, W. Wang, Adv. Opt. Mater. **13**, 2402650 (2025)
35. G. Hu, B. Xu, A. Wang, Y. Guo, J. Wu, F. Muhammad, W. Meng, C. Wang, S. Sui, Y. Liu, Y. Li, Y. Zhang, Y. Zhou, Z. Deng, Adv. Funct. Mater. **31**, 2011191 (2021)
36. J.J. McKinnon, D. Jayatilaka, M.A. Spackman, Chem. Commun. 37, 3814–3816 (2007)
37. D. Prasad Panda, D. Swain, A. Sundaresan, Inorg. Chem. **61**, 11377–11386 (2022)
38. T. Chang, Y. Dai, Q. Wei, X. Xu, S. Cao, B. Zou, Q. Zhang, R. Zeng, ACS Appl. Mater. Interfaces. **15**, 5487–5494 (2023)
39. R. Zhang, H. Xie, W. Liu, K. Zhan, H. Liu, Z. Tang, C. Yang, ACS Appl. Mater. Interfaces. **15**, 47238–47249 (2023)
40. X.T. Liu, C.D. Ge, Z.Q. Yang, Y.L. Song, A.R. Wang, Y.F. Kang, B. Li, Q.F. Dong, Adv. Opt. Mater. **9**, 2100862 (2021)
41. D.P. Panda, D. Swain, R. Raghunathan, A. Sundaresan, Chem. Mater. **36**, 11, 5698–5708 (2024)
42. J.-F. Liao, Z. Zhang, L. Zhou, Z. Tang, G. Xing, Angew Chem. Int. Ed. **63**, e202404100 (2024)
43. B. Li, J. Jin, X. Liu, M. Yin, X. Zhang, Z. Xia, Y. Xu, ACS Mater. Lett. **6**, 1542–1548 (2024)
44. G.H. Tan, Y.N. Chen, Y.T. Chuang, H.C. Lin, C.A. Hsieh, Y.S. Chen, T.Y. Lee, W.C. Miao, H.C. Kuo, L.Y. Chen, K.T. Wong, H.W. Lin, Small **9**, 2205981 (2023)
45. W. Jia, Q. Wei, S. Ge, C. Peng, T. Huang, S. Yao, Y. Tian, T. Chang, R. Zeng, B. Zou, J. Phys. Chem. C **125**, 18031–18039 (2021)
46. C. Li, Z.S. Luo, Y.L. Liu, Y. Wei, X. He, Z.W. Chen, L.M. Zhang, Y.L. Chen, W. Wang, Y.J. Liu, X.Y. Chang, Z.W. Quan, Adv. Opt. Mater. **10**, 2102746 (2022)
47. W. Li, Z. Zhou, C. Wang, Y. Li, S. Kurosawa, G. Ren, X. Ouyang, Y. Wu, Adv. Sens. Res. **2**, 2200083 (2023)
48. H. Cheng, X. Hu, C. Cao, H. Xu, X. Liu, X. Li, H. Wang, K. Huang, W. Yang, D. Wang, R. Xie, Mater. Today Chem. **42**, 102343 (2024)
49. M. Wang, X. Wang, B. Zhang, F. Li, H. Meng, S. Liu, Q. Zhao, J. Mater. Chem. C **11**, 3206 (2023)
50. K. Li, W. Zhang, L. Niu, Y. Ye, J. Ren, C. Liu, Adv. Sci. **10**, 2204843 (2023)

Authors and Affiliations

Xiaokang Zheng[1,2,3] · Zikang Li[2] · Peng Tao[2,3] · Hua Wang[1,4] · Lijie Zhang[5] · Wai-Yeung Wong[2,3]

✉ Peng Tao
pengtao@polyu.edu.hk

✉ Hua Wang
wanghua001@tyut.edu.cn

✉ Wai-Yeung Wong
wai-yeung.wong@polyu.edu.hk

[1] MOE Key Laboratory of Interface Science and Engineering in Advanced Materials, Taiyuan University of Technology, Taiyuan 030024, P. R. China

[2] Department of Applied Biology and Chemical Technology and Research Institute for Smart Energy, The Hong Kong Polytechnic University, Hung Hom, Hong Kong, P. R. China

[3] The Hong Kong Polytechnic University Shenzhen Research Institute, Shenzhen 518057, P. R. China

[4] College of Textile Engineering, Taiyuan University of Technology, Jin Zhong 030600, P. R. China

[5] Zhejiang International Joint Laboratory of Optical Functional Materials, Institute of New Materials & Industry Technology, Wenzhou University, Wenzhou 325000, P. R. China